energy&fuels



Combustion

# INFLUENCE OF ASPHALTENE CONCENTRATION ON THE COMBUSTION OF A HEAVY FUEL OIL DROPLET

Abdulrahman Khateeb, Ayman M. Elbaz, Paolo Guida, and William L. Roberts

*Energy Fuels*, **Just Accepted Manuscript** • DOI: 10.1021/acs.energyfuels.8b03260 • Publication Date (Web): 16 Nov 2018



ACS Publications

is published by the American Chemical Society. 1155 Sixteenth Street N.W., Washington, DC 20036

# INFLUENCE OF ASPHALTENE CONCENTRATION ON THE COMBUSTION OF A HEAVY FUEL OIL DROPLET

**Abdulrahman A. Khateeb[a*], Ayman M. Elbaz[a], Paolo Guida[a], William L. Roberts[a]**

[a]Clean Combustion Research Center, King Abdullah University of Science and Technology,
Thuwal, 23955-6900, Saudi Arabia.

*Corresponding author e-mail: abdulrahman.khateeb@kaust.edu.sa

## Highlights

- Thermogravimetric analysis of heavy fuel oil samples at different asphaltene concentration is discussed.
- The influence of high asphaltene concentration on the droplet burning stages is illustrated.
- The relation between the droplet ignition delay time and droplet size is discussed at different asphaltene concentration.
- The effect of asphaltene concentration on the droplet evolution with time is measured.

## Keywords

*Asphaltene, Burning stages, Heavy fuel oil, Thermogravimetric analysis.*

## Nomenclature

| | |
|---|---|
| $A$ | *frequency factor* |
| $E$ | *activation energy* |
| $k$ | *rate constant* |
| $n$ | *reaction order* |
| $R$ | *universal gas constant* |
| $t$ | *time* |
| $T$ | *absolute temperature* |

| | |
|---|---|
| *wt%* | *weight percentage* |
| $\alpha$ | *fraction decomposition* |
| *API* | *American petroleum institute* |
| *ASTM* | *American society for testing and materials* |
| *DTG* | *differential thermogravimetric* |
| *FD* | *fuel decomposition* |
| *FT-ICR* | *Fourier transform ion cyclotron resonance* |
| *GDT* | *glowing delay time* |
| *HFO* | *heavy fuel oil* |
| *HTO* | *high-temperature oxidation* |
| *IDT* | *ignition delay time* |
| *Le* | *Lewis number* |
| *LTO* | *low-temperature oxidation* |
| *NMR* | *nuclear magnetic resonance* |
| *Slpm* | *standard liter per minute* |
| *TGA* | *thermogravimetric analysis* |

**Abstract**

Heavy fuel oils consist of a blend of middle distillates, mainly diesel fuel, and heavy oil residuals. Varying the fraction of the mixture changes the weight percentage of the asphaltene in the heavy fuel oil (HFO) sample. Asphaltene is a very high molecular weight complex component in the fuel which increases the fuel viscosity, surface tension, and chemical reaction rate. Here, we investigate the influence of high asphaltene concentration on the combustion of a single HFO droplet. In this experimental work, we used the thermogravimetric analysis (TGA) and the suspended droplet techniques. We tested HFO samples containing asphaltene at 8, 16, 24 wt% (HFO8, HFO16, and HFO24). The TGA result shows a residual amount of approximately 2.4 wt% of the HFO24 compared to no residuals for the HFO8 at the end of the process. The suspended droplet technique results reveal the following seven consecutive burning stages for the entire burning process of the liquid and solid phases: 1) pre-heating, 2) flame startup, 3) inner evaporation, 4) thermal decomposition, 5) solidification, 6) coke pre-ignition, and 7) smoldering. The temperature range of the various burning stages is seen to be independent of both the concentration of the asphaltene and the initial size of the droplet. On the other hand, both the total burning time and ignition delay time become longer by 40% and 26% respectively as the content of the asphaltene increases from 8 to 24

wt% in the HFO sample. The evolution of the droplet's size in time shows that the maximum size of the droplet becomes larger by a factor of 2 for the HFO24 compared to the HFO8 sample.

## 1. Introduction

As the demand for hydrocarbon fuels continues to increase rapidly, oil production industries and consumers are paying considerable attention to the dynamic performance and reliability of the combustion process of these fuels. Heavy fuel oil (HFO) has generated increasing interest due to its lower costs, higher durability and heat efficiency compared to similar conventional light oils. Since 2015, HFO market prices have remained approximately 30% lower than crude oil prices [1]. Additionally, the HFO products from a gasification process, mainly CO and $H_2$, can be primarily used in power generation systems with lower emissions [2-4]. The use of different HFO methodologies, such as the gasification process, besides the projected fuel prices, indicates a promising consumption of the heavy fuel oil resources for small-scale power generation systems [5]. However, the use of HFO is facing many challenges due to its negative impacts on the environment, resulting mainly from the emissions of cenospheres and oxides of sulfur. Additionally, HFO has harmful corrosive effects on the equipment used in power generation systems, due to its high content of sulfur. For these reasons, the use of HFO as a source of energy has drastically decreased after reaching the peak in the late of 1970s [5].

The complete combustion of the HFO requires the complete burning of the volatile constituents, in addition to the coke residues. Otherwise, incomplete combustion

of the fuel occurs and thus is more likely to generate soot and coke particles. The poor carbon efficiency of HFO leads to a significantly higher amount of pollutant emissions in the surrounding environment, compared to light fuel oils [6 7]. The composition of heavy fuel oils can vary greatly; as any HFO consists mostly of a blend of middle distillates, mainly diesel, and a heavy oil residual. Varying the fraction of the middle distillate plays a critical role on the key properties such as viscosity, surface tension, and content of asphaltene, all of those being determinant factors for the HFO combustion characteristics. This concept forms the primary objective of this study, that is, to generalize the effects of the concentration of asphaltene on the burning stages of the heavy fuel oil.

In industrial processes, the HFO is atomized via steam assisted or air blast nozzles. Most of the literature is therefore based on sprays of fuel oils. The goal of such studies is to collect qualitative and quantitative information about the combustion process and burning stages of the fuel droplets [2 5 8-10]. Even though generating a spray is implemented in almost every industrial application, the single suspended droplet technique is a powerful tool that permits the simplification of the problem and studies the effect of different technologies, such as the modification of the asphaltene content or the addition of water, on the burning process. Therefore, studying a single suspended droplet is used to explore the fundamental combustion characteristics of heavy fuel oils.

Previous research studies on a single suspended droplet revealed various HFO combustion stages that can be divided into physical and chemical phenomena, both taking place in liquid and gas phase [10-14].

Moreover, the single droplet technique has been used to study the ignition and combustion characteristics of a wide range of different fuel samples. For example, heavy oil residues [15], diesel and biodiesel fuels [16-18], and slurry fuels [19 20]. Another group of researchers used the suspended droplet technique to investigate the use of non-organic dopants on waste-derived fuel and coal-water slurry to prepare compositions which are environmentally friendly and relatively high in power efficiency [21-24].

Braide *et al.*[6] successfully divided the liquid phase into two steps: preheating and flaming, and Baert *et al.*[25] showed that the flaming step was a complicated process involving pyrolysis and a polymerization chemical reaction. The pyrolysis produces soot around the droplet, and the polymerization forms a solid particle at the end of the liquid phase. Additional studies by Ikegami *et al.*[9] suggested that the liquid phase could be subdivided into four consecutive stages: pre-heating, evaporation, cracking, and polymerization towards coke residuals. For more than 40 years, the solid phase was considered as a one-step oxidization process. More recently, it has been shown to be composed of two steps, glowing and smoldering [5], and that these stages are mainly

affected by the fuel composition, droplet size, and combustion environment around the droplet. Asphaltene is a very complex component in the heavy fuel oil consisting of aromatic and naphthenic rings linked by chemical bonds, resulting in a high fuel viscosity and surface tension [26].

One of the main causes of the formation of a cenosphere is the presence of asphaltene. The cenosphere is the name given to the hollow carbonaceous spheres formed during the combustion of heavy fuel oil droplets [27]. Several studies using the HFO suspended droplet technique [2 5 9 10], showed variable weight percentage of asphaltene ranging between 3 and 17 wt% (Table 1). In our current study, we tested HFO samples with a higher percentage of asphaltene reaching up to 24 wt%.

**Table 1:** Summary of the weight percentage of asphaltene in heavy fuel oils from the related studies using the suspended droplet technique.

| **Authors (Year)** | **Asphaltene wt%** | | | |
|---|---|---|---|---|
| Bartle *et al.* (**2013**) [2] | 3 | 6 | 9 | 12 |
| Ikegami *et al.* (**2003**) [9] | 11 | 17 | - | - |
| Xu *et al.* (**2002**) [5] | 11 | 17 | - | - |
| Villasenor *et al.* (**1999**) [10] | 13 | 17 | - | - |
| Current study | 8 | 16 | 24 | - |

The content of asphaltene can be adjusted by varying the fraction of the light oil blended with the HFO. As the demand for light oil cuts increases, HFOs will be blended

with a lower fraction of light oils, which, in turn, would increase the percentage of the concentration of asphaltene. Therefore, in compliance with the future economic demand in both light and heavy fuel oils, HFO with higher content of asphaltene is expected to be used in power generation systems [5]. With this in mind, we investigate the influence of high asphaltene concentration through the thermogravimetric analysis and the burning stages of suspended droplets using HFO samples with 8, 16, and 24 weight percent of asphaltene. The main goal of this study is to help modelers, and burner designers better understand the influence of a high concentration of asphaltene on the burning process, and ultimately increase the HFO combustion efficiency while reducing maintenance expenses.

## 2. Experimental procedure

A heavy fuel oil (HFO) sample collected from the Shuaiba power plant in Saudi Arabia was tested experimentally, using the suspended droplet technique. HFO8, the base oil sample containing approximately 8 wt% asphaltene, was used as a reference. Its physical properties and elemental compositions are presented in Table 2. Two other HFO samples were prepared, one containing 16 wt% in asphaltene (HFO16) and the other 24 wt% (HFO24). These two samples of higher concentration of asphaltene were prepared in our laboratory, where the asphaltene component was extracted from a portion

of the base oil, HFO8, following the ASTM D3279 standard separation process for asphaltene. The HFO8 sample was treated with n-heptane to separate the asphaltene from the HFO sample. HFO8 was added to n-heptane at a 1: 70 weight ratios and the mixture was subsequently stirred for one hour at 60 °C, followed by three hours at ambient temperature. The solution was then left untouched overnight, before filtering. A filtering pad was used under vacuum to separate and extract the asphaltene component from the mixture. The extracted asphaltene was subsequently left in an oven at 90 °C to dry out the remaining n-heptane moisture. It was then added, by weight percentage, to the base oil HFO8 to prepare the HFO16 and HFO24 samples.

**Table 2:** HFO8 physical properties and compositional data.

| **Physical properties** | **Units** | **Results** |
|---|---|---|
| Density at 288 K | $kg/m^3$ | 970.5 |
| Specific gravity (60/60 °F) | - | 0.9711 |
| Kinematic viscosity at 40 °C | cSt | 618 |
| **Compositional data** | | |
| Sulfur | mass% | 3.3% |
| Asphaltene content | wt% | 8.2% |
| Vanadium | mg/kg | 18.0 |
| Nickel | mg/kg | 11.0 |
| Sodium | mg/kg | 3.4 |
| Zinc | mg/kg | <1.0 |
| Lead | mg/kg | 0.4 |
| Potassium | mg/kg | 0.1 |
| Carbon | mass% | 85.0% |

| | | |
|---|---|---|
| Hydrogen | mass% | 10.9% |
| Oxygen | mass% | 0.03% |
| Nitrogen | mass% | 0.24% |
| **Heating values** | | |
| Higher heating value | BTU/IB | 18258 |
| Lower heating value | BTU/IB | 17255 |

Before conducting suspended droplet experiments, the thermal oxidation behavior of the HFO8 and HFO24 samples was investigated under non-isothermal thermogravimetric (TG) conditions. For the various content of asphaltene, thermogravimetric data were used to perform kinetic calculations. For a given content of asphaltene, the HFO sample was studied using different techniques including thermogravimetric and differential thermogravimetric (TG/DTG), Fourier transforms Ion cyclotron resonance (FT-ICR) mass spectroscopy, and nuclear magnetic resonance (NMR) spectroscopy [28-30]. Thermal analysis techniques have been used to investigate the combustion characteristics of different fuel samples [30-35]. The first application of the thermo-analytical method to study the combustion of crude oil was applied by Tadema [36]. Subsequently, different research groups have this used the same methodology of TGA to evaluate the combustion, pyrolysis kinetic parameters of different fuel samples, for example, HFO [31], individual oil fractions [32 33 37], medium and heavy crude oil [34].

Recently, with the TGA data, the kinetic parameters of Chinese HFO sample were evaluated using the distribution activation energy method [35]. In our study, the thermogravimetric analysis (TG/DTG) was conducted using a Mettler Toledo TGA/DSC (thermogravimetric analysis/differential scanning calorimetry) instrument. This instrument was used to measure the sample weight loss for a wide range of temperature (20 – 1100 °C), at a high resolution of 0.1 µg. The instrument was equipped with a GC 200 gas controller and an auto-sampler. For each experiment, a sample of approximately 10 mg was weighted and placed inside an $Al_2O_3$ crucible. Pure air at a 50 mL/min flow rate was used for the experimental combustion tests, whereas nitrogen gas was used at a 25 mL/min flow rate for purging. Experiments were performed, at a heating rate of 5 °C/min over a 25 – 1000 °C temperature range, under non-isothermal conditions. Before each experiment, the TG analyzer was tested and calibrated using a calcium oxalate monohydrate standard. A blank test was conducted before each experiment to correct for the buoyancy effects, with the same crucible as that used for the TG analysis.

Additionally, to ensure the reproducibility of the results, tests were repeated three times. The main goals of these experiments were to investigate the effects of the asphaltene concentration on the thermal oxidation behavior. Consequently, an Arrhenius

model was applied to the TG/DTG non-isothermal data to predict the apparent activation energy for the two samples HFO8 and HFO24.

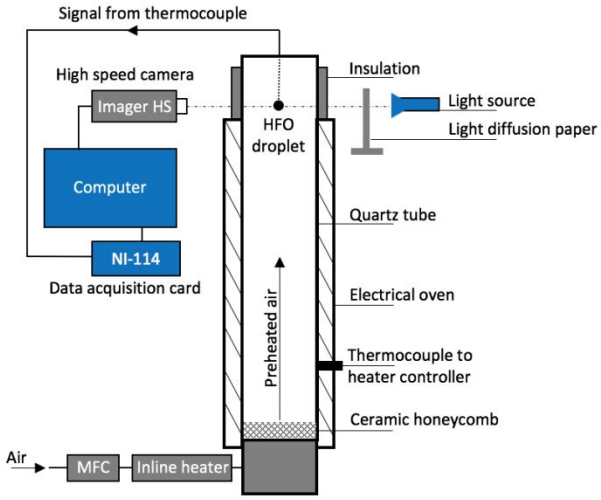


**Figure 1:** Schematic of the experimental setup presenting the main equipment.

Figure 1 shows a schematic of the suspended droplet experimental setup. To support the droplet and to also measure its internal temperature, we used a type S thermocouple made of platinum (Pt) and Platinum-rhodium (Pt-Rh, 13 wt% Rh) wires with a diameter of 75 µm. A vertical quartz tube (inner diameter = 134 mm, and length = 750 mm) was placed inside a vertically oriented cylindrical furnace (Lindberg/blue, HTF55000 series) with control consoles from the standard Lindberg 58000 series. An inline heater (Sylvania heater, F074719, 8000 Watt) was used to preheat the convective air stream flowing inside the quartz tube. The preheated air was supplied from the bottom of the furnace, passing through a ceramic honeycomb, to ensure a uniform air distribution around the droplet. At the droplet location, the air flow rate setting point is

kept at 20 slpm, yielding a velocity of 8.2 cm/s, and the diameter is kept constant, at a set value between 720 and 750 μm. Then, the suspended droplet was placed into the heated air stream that is flowing through the quartz tube. A micro syringe containing the heavy fuel oil sample was used to hang the droplet on the thermocouple bead. The syringe was filled with the quantity corresponding to one droplet only, to control the droplet size. An image analysis MATLAB code was developed to measure the size of the droplet at the beginning of the experiment, and to track its evolution in time. This code can identify the equivalent droplet diameter, as it transformed high-speed images into a binary matrix based on the color gradient measured from the RGB matrix. The gradient was then compared with a threshold that allowed us to discriminate among the phases. The binary matrix of the droplet obtained from this procedure was then normalized using the area of the first image. This procedure generated a value corresponding to the normalized squared diameter. This procedure is important in measuring the droplet size since the droplet did not remain spherical during evaporation, but its shape was altered both by the influence of the thermocouple and the micro-explosive behavior. The uncertainty associated with this procedure was directly related to not taking into account the third dimension.

Moreover, the noise of the captured images created an experimental uncertainty, in the order of one pixel. A 2-D translation system controlled the thermocouple stem movement inside the furnace through a side channel in the quartz tube. This allowed the droplet burning location inside the furnace to stay in a fixed stable position, and for the camera imaging to not show variations in the position of the droplet. An air-cooled shield surrounding the thermocouple carried the droplet until it reached the reaction position with the hot air stream to reduce the heat transfer from the heated air to the heavy fuel oil droplet during the insertion of the droplet inside the furnace. Prior to experiments, the radial temperature readings of the heated co-flow air were recorded in a range of 25 mm radius around the central position, showing a uniform temperature distribution of 950 K. The temperature was recorded using an NI114 data acquisition card, at a 14 Hz sampling rate, while droplet images were acquired through a high-speed camera (Imager HS), at a 1000 frame per second, capturing all the combustion stages.

## 3. Results and discussion

### 3.1 Thermogravimetric analysis

The heavy fuel oil combustion process involved several physical and chemical reactions. The description of the combustion behavior is complex because it involves a wide variety of hydrocarbons having boiling temperatures within a wide range from 160 to 700 °C. The presence of heavy hydrocarbons leads to liquid phase reactions such as pyrolysis and polymerization. The lighter fraction (e.g., diesel fuel) commonly used to reduce the viscosity of the fuel and to reduce the ignition delay time (IDT) corresponded to approximately 40 wt% of the HFO. Figure 2 shows TG data obtained during the combustion of the two samples HFO8 and HFO24, with their TG/DTG curves and combustion stages shown in Fig. 2b and Fig. 2c respectively.

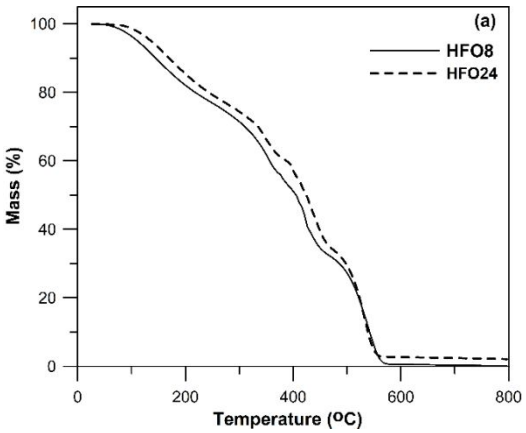

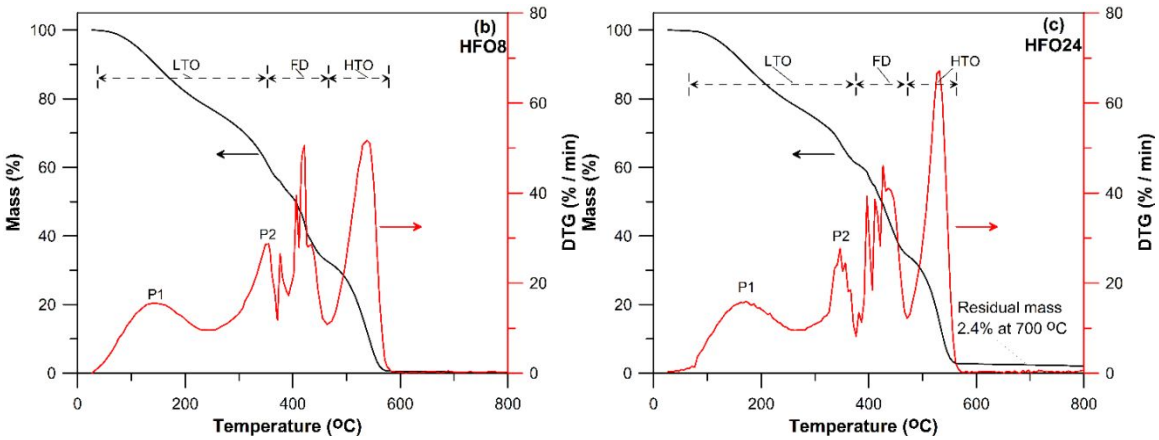


**Figure 2**. (a) Non-isothermal thermogravimetric data for HFO8 and HFO24 samples, (b) TG/DTG combustion curve of the HFO8 sample, and (c) TGA/DTG combustion curve of the HFO24 sample, all at a heating rate of 5 ºC/min

As indicated in Fig. 2, the sample with the highest content of asphaltene, HFO24, led to a time delay of the sample mass reduction; it showed that there was no further apparent thermal degradation in the HFO24 sample beyond a temperature of approximately 580 ºC. A residual amount of approximately 2.4 wt% was found at 700 ºC (Fig. 2), whereas, for the raw sample, no residue was obtained at the end of the process. A close inspection of the TG/DTG plots presented in Fig. 2b and Fig. 2c highlighted three distinct regions from the DTG, in the oxidation of both samples. These three regions correspond to 1) low-temperature oxidation (LTO), 2) fuel decomposition (FD), and 3) high-temperature oxidation (HTO). In the LTO region, the fuel was heated and started to volatilize. Different processes belonged to this stage, with a major contribution coming from the evaporation of the light fraction, similarly to the commercial

diesel cut. In both samples, the evaporation occurred in two consecutive steps, revealed by the two peaks in the DTG profile. After a mass reduction of approximately 1 wt%, a smooth continuous decrease in the TG curve was observed, indicating a rapid mass loss. The DTG profile reached a peak value, defined as P1, at a temperature of 147 °C for the HFO8 sample and 172 °C for the HFO24. Up to this point, the low boiling gases left out the fuel, but as the temperature further increased, the rate of volatilization decreased, reaching a minimum value after P1, first for the HFO8, and then for the HFO24 sample, at a higher temperature. The second phase of the devolatilization started from the minimum point on the DTG curve (after P1) when the vaporization started to become more rapid again. This showed a faster decrease in the sample mass degradation than the first volatilization stage, reaching a peak point P2 on the DTG curve, at a temperature of 352 °C for the HFO8, and 347 °C for the HFO24 sample. The occurrence of two different volatilization stages was attributed to the polymerization reactions forming a layer on the surface of the sample, resulting in a limitation of the mass transfer retaining the hydrocarbons with a higher boiling point. This phenomenon (called the skin-like effect) was revealed in previous studies [39]. The side chains of the heavy compounds were subsequently split and subjected to the low-temperature oxidation [27 30 40].

During the FD phase, oxidation reaction between the gases generated from the previous step (LTO region) continued with the liquid hydrocarbon phase. The higher temperature within this zone and the existence of heavy metals such as Vanadium and Nickel (see Table 2 for oil compositional and elemental analysis) catalyzed the liquid phase oxidation [41]. The catalytic effect of the metals explained the steep decrease in the mass of the sample observed in the FD region. In this region, the DTG plots revealed sharp fluctuations (up and down), corresponding to a breakdown of the skin-like shape by the volatile fractions formed in the LTO region. The FD region ranged from 371 to 466 $^{o}$C for the HFO8, and from 376 to 472 $^{o}$C for the HFO24 sample, with more fluctuations for the HFO24 sample, indicating a high resistance for mass transfer. As the FD region came to an end, the rate of mass degradation decreased again, due to a mass transfer resistance by the formation of carbonaceous particles. This process was found to be similar to the creation of shell type structures (cenosphere) during the combustion of the HFO droplets [27 42 43]. We expected to observe a high ratio of carbon to hydrogen residues at the end of the FD region with holes and cracks within the sample due to the emission of gases through the shell-like surface, similarly was observed in previous experimental studies [2]. The high-temperature oxidation, HTO, was the final region of the combustion of the HFO sample and it extended from 466 $^{o}$C to 577 $^{o}$C

for the HFO8 sample, and from 472 °C to 566 °C for the HFO24 sample. Within this region, the reactions with the oxygen occurred heterogeneously on the surface of the formed shell. In this stage, the oxygen diffused into the shell inside the surface holes and cracks showing the highest rate of mass degradation. As a result of the higher content of asphaltene, for the HFO24 sample and at the end of the HTO region, nearly 97.5 wt% of the initial mass was lost, leaving a residual mass of 2.5 wt% at 700 °C. A value of nearly 0.1 wt% was found at the same temperature, for the HFO8 sample. The cenosphere size was found to be directly proportional to the initial asphaltene concentration [27]. Thus, we found the residual ash more abundant in the HFO24 sample than in the HFO8. The regions for which reactions occur and the temperature of the peak points, for the two samples, are summarized in Table 3.

**Table 3:** Reaction regions, and the temperature of the peak points of the combustion of the HFO8 and the HFO24 samples at a heating rate of 5 °C/min.

| Sample | LTO | FD | HTO | P1 | P2 | Peak at HTO |
|---|---|---|---|---|---|---|
| **HFO8** | 41-371 | 371-466 | 466-577 | 147 | 352 | 542 |
| **HFO24** | 72-376 | 376-472 | 472-566 | 172 | 347 | 532 |

A kinetic study of the HFO combustion is a challenging problem due to the complexity of the fuel composition and the variety of physical reactions associated with the combustion process, and which makes this topic different from a purely chemical

problem. The wide range of molecular weights and boiling points of the constituents of HFO makes the combustion process complicated, and therefore, the fuel non-isothermal weight loss kinetics is a complex phenomenon. This combustion complexity is due to the multiple simultaneous reactions; hence, the evaluated kinetics parameters should be regarded as apparent kinetic values representing complex parallel and serial reactions. In this work, we assumed that the mass transfer constraints have a negligible effect on the reaction progress because of the small size of the sample, and there is an excess of purge gas supply around the sample crucible. We also assumed that the rate of mass loss of the initial sample is only dependent on the rate constant where the mass of the sample remains with a reaction order of unity and temperature. Therefore, it is reasonable to assume that the first-order rate equation can describe the non-isothermal combustion [44]. In the following analysis, we assumed that the limitations on the mass transfer had no clear effect on the reaction behaviors [44]. Here, we aimed to investigate the effects of asphaltene concentration on the kinetic parameters. The Arrhenius model [31-38] [45] was used to estimate the apparent activation energy. The kinetic data calculation was based on the following kinetic equation, where $\alpha$ is the sample fraction decomposition at any time $t$, $k$ is the rate constant, and $n$ is the reaction order.

$$\frac{d\alpha}{dt} = k(1 - \alpha)^n \quad (1)$$

The temperature dependence of $k$ is expressed by the following Arrhenius equation, where $A$ is the frequency factor (1/s), $E$ is the activation energy (kJ/mol), $R$ is the universal gas constant (J/mol. K), and $T$ is the absolute temperature (K).

$$k = Aexp\left(-\frac{E}{RT}\right) \quad (2)$$

The Arrhenius model assumes that the rate of mass loss of the total sample depends only on the rate constant, the remaining mass sample, and the temperature. Accordingly, the Arrhenius type kinetic model takes the following form assuming the first order of reaction, where $^{dw}/_{dt}$ is the rate of mass change (g/s).

$$\log \frac{^{dw}/_{dt}}{w} = \log A - \frac{E}{2.303RT} \quad (3)$$

We applied the Arrhenius model to the TG/DTG presented in Fig. 2. by plotting log [( $^{dw}/_{dt}$)/ $w$] on the vertical axis versus 1/T on the horizontal axis; the activation energies of the HFO samples within the LTO and HTO regions were obtained via equating the slope of the straight line to E/2.303 RT (Fig. 3), both for the HFO8 and the HFO24 samples. The estimated activation energy is listed in Table 4, and the Arrhenius model is shown in Fig. 3.

**Table 4:** Activation energy obtained for different reaction regions of HFO8 and HFO24 samples.

| **Sample** | **Arrhenius model, $E$ (kJ/mole)** | | |
|---|---|---|---|
| | LTO region | | HTO |
| | LTO up to P1 | LTO up to P2 | |
| **HFO8** | 26 | 39 | 177 |
| **HFO24** | 38 | 50 | 238 |

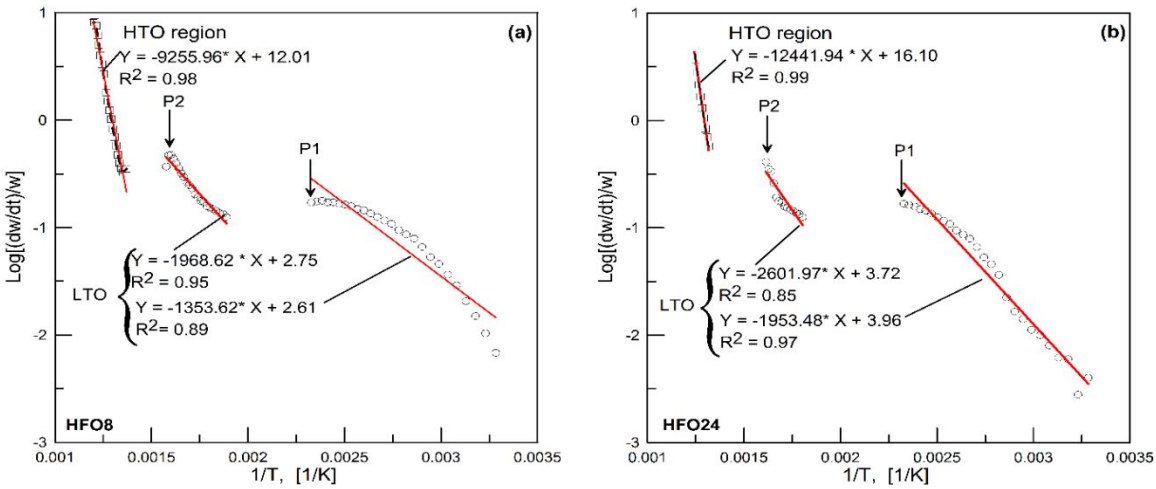


**Figure 3.** Arrhenius model to evaluate the apparent activation energy in the LTO and HTO regions for (a) HFO8 sample, and (b) HFO24 sample.

As indicated by the TG/DTG curves in Fig. 2, the LTO regions have two stages of volatilization for the low and high boiling volatile gases, leaving the sample up to the peak points P1 and P2. Accordingly, as illustrated in Fig. 3, two straight lines could fit the Arrhenius data model for the low and high boiling gases, in the LTO region. We found that, for both samples, the second stage of volatilization, during which the high boiling temperature, volatiles (aromatics) were released up to the peak point P2, had apparent activation energy higher than in the first stage (which ends at the peak point P1). At higher temperatures (Table 4), the estimated value of the activation energy value was higher for the HTO region than for the LTO evaporation phases. This indicates that the three distinct regions, LTO, FD, and HTO have different activation energies due to the change in the combustion mode. In the LTO region, the reaction occurred in a

heterogeneous liquid phase, with two consecutive stages of low and high boiling volatiles. The phase subsequently became a homogeneous gas phase in the FD region during which the fuel compounds for the HTO region were formed. In the high-temperature oxidation region, the hydrocarbon/char reactions played a dominant role. As shown in Fig. 3, the increase in asphaltene contents led to an increase of the activation energy. Slightly higher activation energy in the LTO region of the HFO24 compared to the HFO8 as the oxidation reaction of the asphaltene is slow in this region [46]. However, as the concentration of asphaltene increased, a significant increase in the activation energy was observed in the HTO region during which the phase of the reaction changed into solid. Similar observations were made for the activation energy across the different combustion stages [34 46]. It was also observed that the apparent activation energy increased as the API gravity of the oil was decreased, due to the presence of higher asphaltene content [34].

### 3.2 Burning stages

The burning stages of a heavy fuel oil droplet were illustrated using the suspended droplet technique, where the initial diameter is approximately 720 – 750 µm. The air stream temperature inside the furnace is set to 950 K, and the co-flow air rate is constant at 20 slpm, giving a velocity of 8.2 cm/s. In previous work [27], the droplet size,

air stream temperature, and air flow rate were extensively investigated to identify the autoignition temperature, using a similar fuel sample and experimental setup. For this study, the experimental parameters were selected, based on our previous work [27], in order to provide the necessary conditions for the autoignition of the droplet. Figure 4 shows the droplet temperature profile, starting from its insertion into the preheated air stream to the end of the solid combustion process and the extinction of the coke. As shown in Fig. 4, the entire burning process of the HFO droplet comprises two phases: a liquid phase followed by a solid phase. The liquid phase combustion was found to be a complex event consisting of several consecutive stages, each of them characterized by distinctive physical and chemical reactions. The solid coke phase represented a period of heterogeneous surface oxidation of the carbonaceous residue 9. Referring to the thermogravimetric analysis, the liquid phase combustion occurs during the LTO and FD regions, while the solid phase combustion occurs during the HTO region. The entire burning process was composed of seven consecutive stages: 1) pre-heating, 2) flame startup, 3) inner evaporation, 4) thermal decomposition, 5) solidification, 6) coke pre-ignition and 7) smoldering.

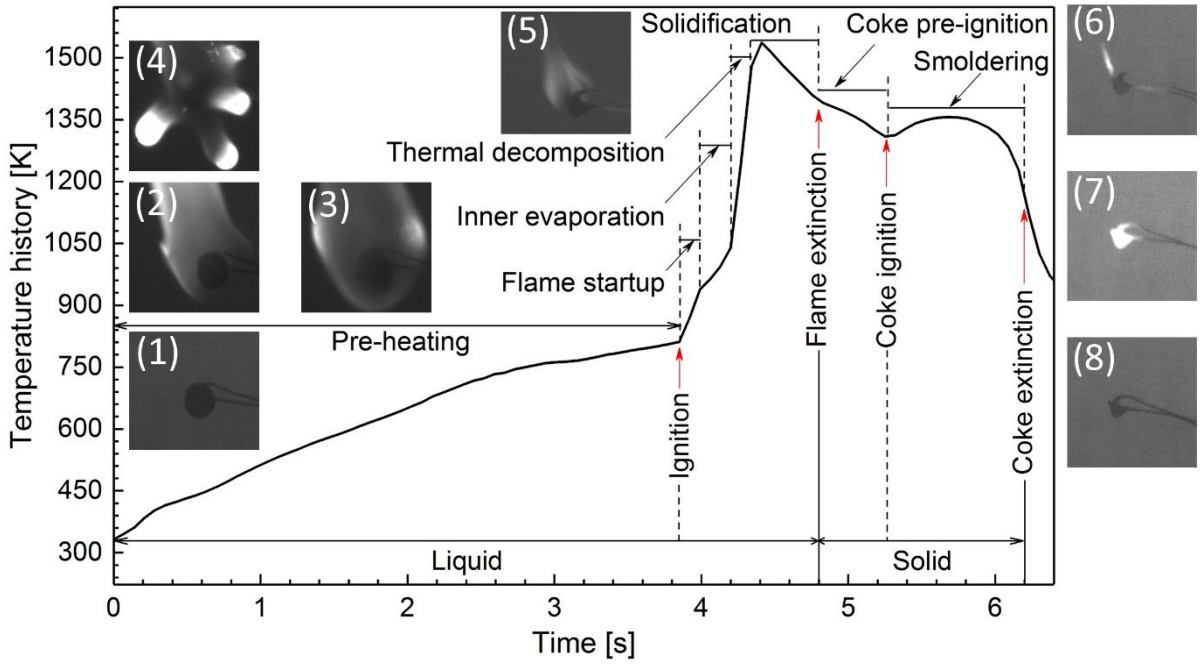


**Figure 4:** Temperature profile of a suspended HFO8 droplet, with an initial diameter of 750 µm, showing high-speed images of the combustion stages. The heated co-flow air temperature is set to 950 K, and the velocity to 8.2 cm/s.

The burning process started with the heating of the particle through convective heat transfer, at this stage, several fluctuations affect the shape of the droplet due to the micro-explosions behavior. Part of the volatile fraction evaporated superficially, but a significant amount was trapped inside the droplet, leading to periodic expansions ending with a 'jet-like' release of both the fuel and the gaseous compounds. Figure 2 shows this behavior by a change in the TGA/DTG slope as a release of low boiling gases around the peak point, P1, in the LTO region at 420 K. After this point, the rate of volatilization decreases while the temperature keeps increasing. This behavior was different from that described by Baert *et al.* [25] who describes a distillation like process,

while, for the HFO, inner evaporation of the light compounds was observed. As discussed in a previous study [2], the weakest bonds of the heavy fuel oil start to break at approximately 625 K, with the heavy molecules of the residual starting to decompose. At this temperature, Fig. 2 shows a peak, P2, on the TGA/DTG curve as a sign of releasing the high boiling gasses. Then, at the FD region, more mass transfer of the gaseous compound escapes from the droplet due to the oil bonds breaking process. The release of the gases is more intense than the at low boiling gases, P1. A flame event started after ignition of the vapor-air mixture and terminated shortly before the solid coke particle starts forming at the end of the solidification stage. When the vapor/air mixture reached critical ignition temperature, the mixture autoignition created a visible flame around the droplet with no splashing or micro-explosion in the first step, Fig. 4 image 2. The ignition delay time, IDT, is defined as the amount of time between the entrance of the fuel droplet in the hot environment and the appearance of the flame. The first sharp rise in the temperature profile revealed the ignition, mainly through the radiative effect of the flame. The calculation of the ignition delay time was performed either by identifying the peak in the first derivative corresponding to the ignition, or by observing the formation of the flame from the high-speed images. In any case, we found that the increase in the temperature profile was a bit delayed, concerning the formation

of the flame, due to the limitation of the time response of the thermocouple. The absolute error associated with measuring the IDT using the images was found to be inversely proportional to the frame rate, 1000 frame/s in the present study. The droplet burning process displayed four distinctive stages, starting from the ignition of the droplet to the flame extinction: the flame startup, the inner evaporation, the thermal decomposition, and the solidification (Fig. 4). The four distinctive stages occur during the FD region causing disruptions and fluctuations to the DTG curve Fig. 2 as a result of the chemical reactions of different species in the heavy fuel oil. During the flame startup stage, the flame gradually developed, featuring a slight swelling of the droplet, indicating that the evaporation process continued with the remaining volatiles and the products of cracking. The diameter grew exponentially, up to more than four times the initial diameter. Ikegami *et al.* [9] related this phenomenon to the Lewis number, *Le*, as per equation 4. The Lewis number is defined as the ratio between the thermal conductivity $\alpha$, and the mass diffusivity $\Gamma$:

$$Le = \frac{\alpha}{\Gamma} \qquad (4)$$

For this type of fuel, the heat transfer rate is greater than the rate of mass transfer, so Le**>>**1 and the volatile species are trapped inside the droplet at high

temperature. Hence these species evaporate and react while the heavier ones, such as asphaltene, form a solid shell. As the evaporation of the light fraction proceeded, the heavier species accumulated on the surface of the droplet. This accumulation leads to a higher resistance to the mass transfer. The inner evaporation started after the flame startup stage and ended with a thermal decomposition occurring during the initial phase of the fuel evaporation, as described by Chen & El-Wakil [47]. During this stage, the temperature increased at a low rate, but the droplet displayed a large swollen, as illustrated in Fig. 4 image 3, due to the release of the high boiling gases. Ikegami *et al.* [9] explained the decrease in temperature rate by thermal cracking, an endothermic process requiring a relatively high amount of energy, as indicated by the activation energy in Table 4. Splashing occurred during the early phase of the inner evaporation stage when the droplet surface viscosity was not high enough to prevent it. At this stage, the flame was very sensitive to the droplet as it swelled and returned to its original size continuously. At the end of this stage, the droplet surface viscosity progressively increased, leading to a higher tendency to have a micro-explosive behavior, as illustrated in Fig. 4 image 4. The next stage, *i.e.,* the thermal decomposition stage, started with a sharp increase in temperature, as a result of the decomposition of the fuel constituents and the production of the volatile gases.

The non-aromatic part produces volatile gases as a result of the thermal cracking, decreasing the molecular weight of the heavy fuel [48]. Consequently, the micro-explosions became more intense and frequent, due to the increase in surface tension caused by the evaporation of superficial volatiles trapping the gaseous inside the droplet. The trapped gases could only escape from the droplet because of the micro-explosive behavior. The droplet subsequently entered the solidification stage, also called the polymerization stage, which represented a transient period between the liquid and solid phases. The DTG curve in Fig. 2 shows this transition occurring at low mass degradation point between the FD and HTO regions. During this transition, the rate of mass degradation was decreased, due to resistance in mass transfer by the formation of carbonaceous particles, as previously described (in the thermogravimetric analysis section). The solidification involved mostly a combination of the aromatic parts. The thermal cracking reduced the heavy fuel molecules to their aromatic nuclei, which are very stable and only began to decompose at 1000 K [48].

The aromatic nuclei either evaporated or recombined to form polymers from the residual components [48]. During this period, the droplet temperature was no longer controlled by the fuel evaporation process, and the droplet reached its maximum temperature, forming a solid particle of coke residue. The flame intensity was then

reduced steadily Fig. 4 image 5. Accordingly, the droplet temperature decreases gradually until the flame became extinct (Fig. 4 (6)), while the solid phase was being initiated. Due to the extinction of the flame, the residue collapsed around the thermocouple bead, to form a cenosphere. The co-flow of air was then able to diffuse to the surface of the coke particle to react. Thus, a significant amount of energy was released during the high-temperature oxidation region, which ended by a glowing of the coke, a final stage called 'smoldering stage' Fig. 4 image 7. This energy is much higher than that in the LTO region as discussed in the thermogravimetric analysis section.

The amount of time from flame extinction to the coke glowing is defined as the glowing delay time, GDT. The smoldering stage takes place to burn the remaining coke particles until quenching occurs, as heat losses exceed the heat generation, leaving unburnt coke. During this stage, the temperature displays a gradual increase to a peak temperature. The droplet lifetime can be calculated as the amount of time between insertion of the droplet into the furnace and the coke extinction Fig. 4 image 8.

### 3.3 Influence of high asphaltene concentration

Figure 5a and the zoomed window in Fig. 5b, compare the droplet temperature histories for the three different samples HFO8, HFO16, and HFO24, featuring the main burning stages. For the three HFO samples, the initial droplet diameter for the tests is

approximately 720 - 750 µm, the air flow temperature is set to 950 K, and the velocity is set to 8.2 cm/s.

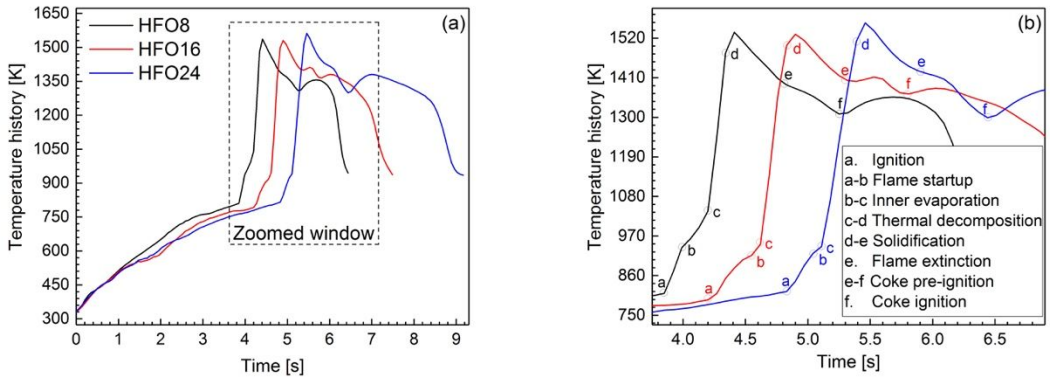


**Figure 5:** (a) Suspended droplet temperature profiles for HFO8, HFO16, and HFO24; (b) zoomed window of the temperature profile showing closely the burning stages. The initial droplet diameter is 750 µm, the airflow temperature is set to 950 K, and the velocity is set to 8.2 cm/s.

Increasing the asphaltene concentration does not affect the range of temperature associated with each combustion stage; it only delays or shifts the start of the droplet ignition and burning stages. For instance, the ignition temperature is almost the same for the three samples, approximately 775 K. However, compared to the HFO8, the ignition of the HFO16, and HFO24 droplets occurred at a later time corresponding to the larger content of asphaltene concentration. This means that a longer duration time of the preheating stage was required for the flame to start up for the HFO24 than the HFO8 (Fig. 6), and this matches the TGA findings. Accordingly, the total burning time of the droplet increased by 40% for the HFO24 compared to the HFO8. A higher

percentage of asphaltene leads to a reduction of the weight percentage of the light components, in particular, since the blending procedure is usually carried out with approximately 40 wt% of lighter cut in the HFO8, the reduction of the diesel-like fraction is about 36.5 wt% for the HFO16 and 33 wt% for the HFO24. Figure 6 summarizes the duration time in seconds, for each burning stage for the three HFO samples.

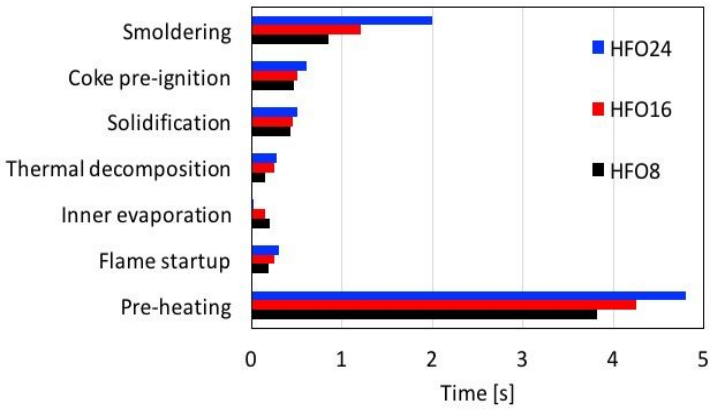


**Figure 6.** Duration time of the seven burning stages for the HFO8, HFO16, and HFO24 droplets related to the temperature profile shown in Fig. 5.

The duration time for each stage is sensitive to the asphaltene concentration as illustrated in Fig. 6. The pre-heating stage contributes most of the combustion process of the droplet with approximately 50% of the total burning time. Increasing the asphaltene concentration increases the pre-heating stage length as the asphaltene increases the droplet viscosity. The second stage, flame startup, also increases with increasing the asphaltene concentration. This is because of creating ignitable environment depends mainly on forming the right mixture between the fuel gasses and hot air during the pre-

heating stage. We found that the length of the flame startup stage is almost double for HFO24 than it is for HFO8 (Fig. 6). On the other hand, the length of the inner evaporation stage has an inverse relationship with the asphaltene concentration. Figure 6 shows that the inner evaporation time dropped from 0.2 seconds, in the HFO8, to 0.025 seconds, in the HFO24. This can be explained by the larger skin-like effect which limits the mass transfer of the inner gases with higher asphaltene concentration. Both thermal decomposition and solidification stages increase proportionally with increasing the asphaltene percentage. Also, the entire solid phase including the coke pre-ignition and smoldering stages increases with increasing the asphaltene percentage. The HFO24 contained heavier components, and therefore induced longer polymerization reactions than the HFO8. Additionally, the residual of the HFO24 was much larger, as shown in Fig. 2, thus, required a longer time for the heterogeneous reaction to be ignited. Accordingly, the coke pre-ignition stage, also called glowing delay time, increased from 0.47 seconds to 0.60 seconds, as we increased the concentration of asphaltene from 8 to 24 wt.% respectively. Furthermore, we observed an increase in the duration of the smoldering stage of the solid particle, from 0.85 seconds for HFO8, to 2 seconds for HFO24 Figs. 6. The coke burnout time, from coke ignition to coke extinction, increased from 15% to 25% of the total droplet's lifetime.

Figure 7 presents high-speed images of the seven different burning stages, for the three samples HFO8, HFO16, and HFO24. The results show qualitative combustion characteristics, similar to those illustrated in Fig. 4. The droplet images at each stage show similar behavior despite the variations in the asphaltene concentration.

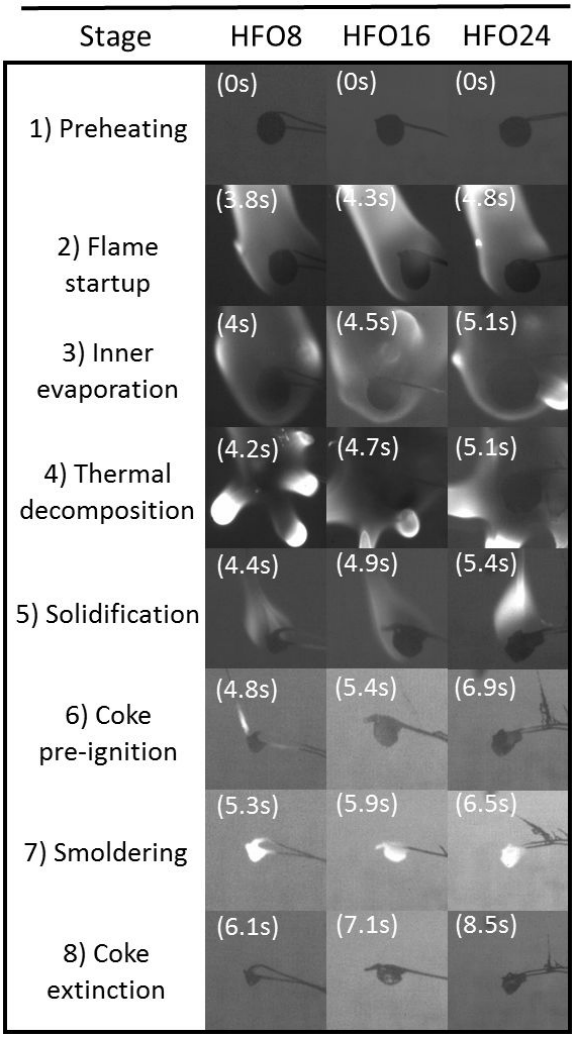


**Figure 7:** Transient images of the HFO8, HFO16, and HFO24 droplets and flames related to the plots in Fig. 5.

During the pre-heating stage Fig. 7 (1), the droplet was preheated in a spherical shape with less surface distortion and more stability for the HFO24 sample. However,

the size of the droplet becomes larger than the original size due to the low boiling gases. In the second stage, flame startup, similar behavior of visible flame was observed in Fig. 7 (2) for the three, although HFO8 experienced the highest increase in temperature during the flame startup stage Fig. 5 (a-b). Very little change was observed between HFO16 and HFO24. Additionally, a steady decrease in the time required for the inner evaporation stage was obtained by increasing the asphaltene concentration Fig. 5 (b-c). The slower rate of the inner evaporation in HFO24 than HFO8 shows a bigger size of the droplet Fig. 7 (3) proportionally with the amount the trapped inner gasses. The thermal decomposition stage Fig. 5 (c-d) occurred at an earlier time for a higher content of asphaltene. This can be explained by the fact that the thermal decomposition and solidification stages are mostly a function of the heavier components, and therefore, excessive micro-explosions occurred with a higher content of asphaltene (Fig. 7 (4)). The effect of increasing the asphaltene on the thermal decomposition stage appeared clearly in the TGA/DTG results (Fig. 2) through more fluctuations during the FD region for the HFO24 than the HFO8. Increasing the concentration of asphaltene led to the formation of bigger coke particles during the solidification stage (Fig. 7 (5-7)), requiring a longer coke pre-ignition and smoldering time Fig. 6. Accordingly, a larger coke particle was left unburnt, Fig. 7 (8), when the content of asphaltene increased from 8 to 24

wt.%. In compliance with the residual mass of 2.4 wt% was obtained for the HFO24 sample, whereas no residue was found for the HFO8 sample. Those experimental results are consistent with the TGA results.

Figure 8 shows the droplet normalized square diameter for the three HFO samples (HFO8, HFO16, HFO24), and a zoomed view of the micro-explosive zone during the pre-heating stage, for the three samples. Tracking the droplet evolution with time is fundamentally important to explore the effect of the asphaltenes on the micro-explosions. This principle helps to characterize fuels with a wide boiling range and to understand the relevant effect on the combustion efficiency [49] [50].

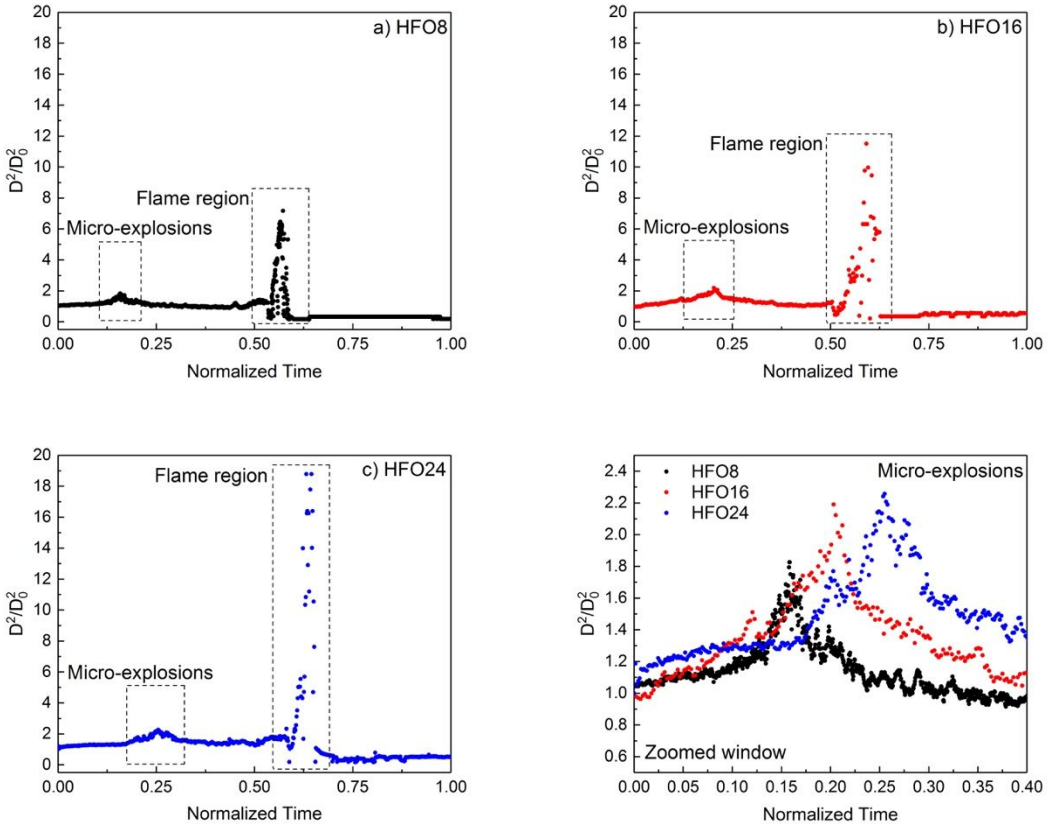


**Figure 8:** Normalized squared diameter for the three samples, a) HFO8, b) HFO16, c) HFO24; with a zoomed view of the micro-explosions during the pre-heating stage.

Increasing the asphaltene content increases the droplet's viscosity and reduces the reactivity of the mixture. The evolution of the normalized squared droplet diameter profile highlighted these features. We observed that the amplitude of the oscillations of the droplet size in the evaporative regions was much more consistent for the sample with the highest content of asphaltene, in comparison with the raw fuel. Oscillations are strictly related to the micro-explosive behavior; as this is because the formation of the bubbles inside the fuel matrix is the step preceding this phenomenon. Samples HFO16

and HFO24 were more capable of restraining the super-heated vapors inside the particles, resulting in a larger peak in the droplet size than the HFO8 [9 51] as indicated in Fig 8. As shown in Fig. 8, the size of the HFO8 droplet is smaller at the end of the micro-explosive step than it was initially, due to the loss in the fuel in the form of micro-satellites. This process is of relevant importance in the industrial sector, particularly for spray combustors, because it generates secondary atomization that improves the evaporation rate and increases the surface area of the fuel in contact with the surrounding atmosphere [51]. A fast consumption of fuel is observed after the ignition Fig. 8 a, b, and c, it corresponds to a drastic reduction of the droplet size followed by a rapid expansion which generates a maximum size that is again proportional to the asphaltene content. The maximum size of the droplet becomes larger by a factor of 2 with increasing the asphaltene concentration from 8 to 24 wt% in the HFO sample, again a symptom of a remarkable capacity of the asphaltene to create a shell and trap the vapors. All the three samples present a disruptive behavior at the end of the combustion stage when the shell collapses releasing the vapors and forming the cenosphere.

### 3.4 Ignition delay time

In this experimental work, we investigate the influence of high asphaltene concentration on the ignition delay time for different droplet initial size. The ignition delay

time was examined as a function of the initial droplet diameter for the HFO8, HFO16, and HFO24 samples. Figure 9 presents the ignition delay time for approximately fifty different droplets for each sample, and for a diameter size ranging from 400 µm and 900 µm.

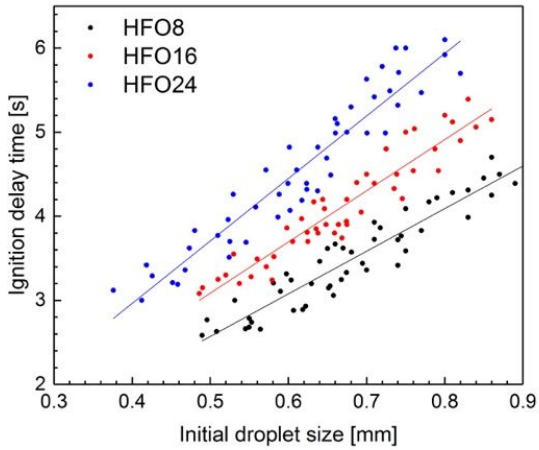


**Figure 9:** Ignition delay time for different HFO8, HFO16, and HFO24 droplet size.

The ignition delay time, IDT, is the time required for the combustible mixture to form around the droplet plus the time necessary for the early stage chemical reactions to ignite the droplet. In our previous work [27], we discussed the required conditions for HFO droplet autoignition to occur. The IDT could be divided into a heat-up time and an evaporation/mixing time. For the present study, the droplet's asphaltene concentration control the ignition delay by a positive linear relationship between the heating time and the droplet size. As shown in Fig. 9, the ignition delay time increases as the diameter of the droplet increases for the three HFO samples. The time delay for the ignition of

the larger HFO droplet is due to the difficulty in forming the air/fuel mixture, which, in turn, leads to the droplet's autoignition. Moreover, the evaporation/mixing time increases with the delay time for samples with a high concentration of asphaltene. We found the droplet ignition delay time to be a function of both the droplet size and the content of asphaltene. For example, the IDT increases by 26% when the asphaltene concentration increases from 8 to 24 wt% in the HFO sample. On the other hand, the temperature of the droplet during the ignition step does not strongly depend on these two parameters.

### 3.5 Experimental error

One of the largest sources of error in the temperature measurements arises from uncertainty in the location of the thermocouple in the droplet. The droplet position on the thermocouple junction changes due to the oscillations of the droplet interface during the combustion process. The temperature measurements obtained is an average of the inner liquid phase temperature except for some instants where the micro-explosions move the droplet leaving the junction uncovered. The characteristic time of these events is much smaller compared to the data acquisition rate by the thermocouple and are effectively averaged out.

The experimental error associated with the interface measurements and tracking is of the same order of magnitude of a single pixel. The major issue is represented by

the fact that the third dimension is completely neglected since the images can observe no depth in the actual experimental setup. The measurements of the normalized square diameter are based on the assumption that the ratio between the surface of the droplet at a certain instant and the original surface has the same ratio between the measured 2-D area and the original area of the droplet.

## 4. Conclusions

The primary purpose of this work was to experimentally investigate the influence of the asphaltene concentration on the combustion of a heavy fuel oil droplet. We tested HFO samples containing asphaltene concentration of 8, 16, and 24 wt%. This work provides quantitative information about the combustion of HFO from the thermogravimetric analysis and the combustion of a suspended droplet.

TGA results have shown that increasing the content of asphaltene from 8 to 24 wt% in the HFO sample delays the mass degradation starting time and leaves a residual of 2.4 wt% at the end of the process. The results have revealed seven burning stages during the complete liquid and solid phases: 1) pre-heating, 2) flame startup, 3) inner evaporation, 4) thermal decomposition, 5) solidification, 6) coke pre-ignition, and 7) smoldering. Increasing the asphaltene concentration increases the duration time of six out of the seven burning stages. The inner evaporation stage, by contrast, decreases

with increasing the asphaltene concentration. For the same droplet size, the total burning time increases by 40% when increasing the asphaltene concentration from 8 to 24 wt%. Likewise, the ignition delay time increases by 26%. On the other hand, increasing the asphaltene concentration does not affect the temperature range of the various burning stages.

The micro-explosive behavior is still present even when increasing the amount of asphaltene inside the mixture up to 24 wt%. The higher asphaltene content leads to a larger maximum size of the droplet over the burning time by approximately a factor of 2 for the HFO24 sample compared to the HFO8. In our future work, we will consider the effects of these phenomena on the spray combustion behavior.

**Acknowledgments**

The research reported in this publication was supported by Saudi Electricity Company (SEC) under grant number RGC/3/3466-01-01 and by King Abdullah University of Science and Technology (KAUST).

## References

(1) Roy, B.; Comer, B. Alternatives to heavy fuel oil use in the Arctic: Economic and environmental tradeoffs; **2017**.

(2) Bartle, K.; Jones, J.; Lea-Langton, A.; Pourkashanian, M.; Ross, A.; Thillaimuthu, J.; Waller, P.; Williams, A. Fuel **2013**, 103, 835-842.

(3) Reyhani, H. A.; Meratizaman, M.; Ebrahimi, A.; Pourali, O.; Amidpour, M. Energy **2016**, 107, 141-164.

(4) Gomez, J.; Mmbaga, J.; Hayes, R.; Toledo, M.; Gracia, F. International Journal of Hydrogen Energy **2016**, 41, 17933-17943.

(5) Xu, G.; Ikegami, M.; Honma, S.; Ikeda, K.; Nagaishi, H.; Takeshita, Y. Combustion science and technology **2002**, 174, 115-145.

(6) Braide, K.; Isles, G.; Jordan, J.; Williams, A. Journal of the Institute of Energy **1979**, 52, 115-124.

(7) Costa, M.; Costen, P.; Lockwood, F. Journal of the Institute of Energy **1991**, 64, 64-76.

(8) Ocampo-Barrera, R.; Villasenor, R.; Diego-Marin, A. Combustion and flame **2001**, 126, 1845-1855.

(9) Ikegami, M.; Xu, G.; Ikeda, K.; Honma, S.; Nagaishi, H.; Dietrich, D.; Takeshita, Y. Fuel **2003**, 82, 293-304.

(10) Villasenor, R.; Garcia, F. Fuel **1999**, 78, 933-944.

(11) Allen, G.; Hocking, W.; Watson, D.; Wild, R.; Street, P. Journal of the Institute of Energy **1984**, 57, 260-265.

(12) Kobayasi, K. An experimental study on the combustion of a fuel droplet. Symposium (International) on Combustion. **1955**, 141-148.

(13) Lightman, P.; Street, P. Journal of the Institute of Energy **1983**, 56, 3-11.

(14) Marrone, N. J.; Kennedy, I. M.; Dryer, F. L. Combustion science and technology **1984**, 36, 149-170.

(15) Zhu, M.; Zhang, Z.; Zhang, Y.; Setyawan, H.; Liu, P.; Zhang, D. Proceedings of the Combustion Institute **2017**, 36, 2475 - 2482.

(16) Zhu, M., Ma, Y., Zhang, D. Proceedings of the Combustion Institute **2013**, 34, 1537 - 1544.

(17) Zhu, M.; Ma, Y.; Zhang, Z.; Chan, Y. L.; Zhang, D. Fuel **2015**, 150, 88 - 95.

(18) Setyawan, H. Y.; Zhu, M.; Zhang, Z.; Zhang, D. Energy **2016**,113, 153 - 159.

(19) Zhu, M.; Zhang, Z.; Zhang, Y.; Liu, P.; Zhang, D. Applied Energy **2017**, 185, 2160 - 2167.

(20) Zhu, M.; Zhang, Z.; Zhang, Y.; Setyawan, H.; Liu, P.; Zhang, D. Proceedings of the Combustion Institute **2017**, 36, 2475 - 2482.

(21) Kuznetsov, G. V.; Vershinina, K. Y.; Valiullin, T. R.; Strizhak, P. A. Fuel Processing Technology **2018**, 179, 407 - 421.

(22) Glushkov, D. O.; Kuznetsov, G. V.; Strizhak, P. A.; Syrodoy, S. V. Energy & Fuels **2018**, 32, 8789-8802.

(23) Nyashina, G. S.; Strizhak, P. A. Environmental Pollution **2018**, 242, 31 - 41.

(24) Egorov, R. I.; Valiullin, T. R.; Strizhak, P. A. Combustion and Flame **2018**, 193, 335 - 343.

(25) Baert, R. Combustion Science and Technology **1993**, 90, 125-147.

(26) Alshareef, A. H.; Azyat, K.; Tykwinski, R. R.; Gray, M. R. Energy & Fuels **2010**, 24, 3998-4004.

(27) Elbaz, A. M.; Khateeb, A. A.; Roberts, W. L. Energy **2018**, 152, 455-465.

(28) Elbaz AM, Gani A, Hourani N, Emwas AH, Sarathy SM, Roberts WL. Energy & Fuels. **2015**, 12, 7825-35.

(29) Abdul Jameel, A. G.; Elbaz, A. M.; Emwas, A.-H.; Roberts, W. L.; Sarathy, S. M. Energy & Fuels **2016**, 30, 3894-3905.

(30) Jameel, A. G. A.; Han, Y.; Brignoli, O.; Telalovic, S.; Elbaz, A. M.; Im, H. G.; Roberts, W. L.; Sarathy, S. M. Journal of Analytical and Applied Pyrolysis **2017**, 127, 183-195.

(31) Ciajolo, A.; Barbella, R. Fuel **1984**, 63, 657–661.

(32) Freitag, P.; Verkoczy, B. Journal of Canadian Petroleum Technology **2005**, 44, 54–61.

(33) Kok, M. V.; Karacan, O. Energy & Fuels **1998**, 12, 580–588.

(34) Kok, M. V. Fuel Processing Technology **2011**, 92, 1026-1031.

(35) Cheng, F.; Cheng, Z.; Qiang, Z.; Desheng, M.; Yue, C.; Hang, J.; Lin, S.; Fei, W. Fuel Processing Technology **2014**, 119, 149–153.

(36) Tadema, H. J. 5th World Petroleum Congress **1959**, 279-287.

(37) Ranjbar, M. Journal of Canadian Petroleum Technology **1995**, 34, 25 - 30.

(38) Kok, M.; Acar, C. Journal of Thermal Analysis and Calorimetry **2005**, 83, 445-449.

(39) Pereira, A. N.; Trevisan, O. V. Journal of the Brazilian Society of Mechanical Sciences and Engineering **2014**, 36, 393-401.

(40) Millington, A.; Price, D.; Hughes, R. Journal of Thermal Analysis and Calorimetry **1993**, 40, 225-238.

(41) Gureyev, A.; Sablina, Z. The Oxidation of Hydrocarbons in the Liquid Phase; Elsevier, **1965**; pp 362-374.

(42) Reddy, V. M.; Rahman, M. M.; Gandi, A. N.; Elbaz, A. M.; Schrecengost, R. A.; Roberts, W. L. Combustion Theory and Modelling **2016**, 20, 154-172.

(43) Urban, D. L.; Dryer, F. L. New results on coke formation in the combustion of heavy-fuel droplets. Symposium (International) on Combustion. **1991**; pp 1437-1443.

(44) Murugan, P.; Mahinpey, N.; Mani, T.; Freitag, N. Fuel **2009**, 88, 1708-1713.

(45) Gundogar, A. S.; Kok, M. V. Fuel **2014**, 123, 59-65.

(46) Ambalae, A.; Mahinpey, N.; Freitag, N. Energy & fuels **2006**, 20, 560-565.

(47) Chen, C.; El-Wakil, M. Experimental and theoretical studies of burning drops of hydro-carbon mixtures. Proceedings of the Institution of Mechanical Engineers, Conference Proceedings. **1969**; pp 95-108.

(48) Garaniya, V.; Goldsworthy L.; McWilliam D. Chemeca **2011**: Engineering a Better World: Sydney (Australia) **2011**, 251.

(49) Rao, D. C. K.; Karmakar, S.; Basu, S. Scientific Reports **2017**, 7, 8925.

(50) Mura, E.; Calabria, R.; Califano, V.; Massoli, P.; Bellettre, Journal Experimental Thermal and Fluid Science, **2014**, 56, 69-74.

(51) Watanabe, H.; Suzuki, Y.; Harada, T.; Matsushita, Y.; Aoki, H.; Miura, T. Energy **2010**, 35, 806-813.